Mechanics of Advanced Composite Structures 5 (2018) 115 – 130

Semnan University

Mechanics of Advanced Composite Structures

journal homepage: http://MACS.journals.semnan.ac.ir

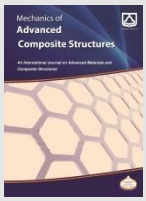

Optimization of infinite composite plates with quasi-triangular holes under in-plane loading

S. A. Mahmodzade Hoseyni, M. Jafari*

Department of Mechanical Engineering, Shahrood University of Technology, Shahrood, Iran, 36199-95161, Shahrood, Iran

PAPER INFO

Paper history:
Received 2016-11-20
Received in revised form 2017-05-28
Accepted 2018-01-30

Keywords:
Infinite orthotropic plate
Quasi-triangular hole
Particle swarm optimization
Analytical solution
Complex variable method

ABSTRACT

This study used particle swarm optimization (PSO) to determine the optimal values of effective design variables acting on the stress distribution around a quasi-triangular hole in an infinite orthotropic plate. These parameters were load angle, hole orientation, bluntness, fiber angle, and material properties, which were ascertained on the basis of an analytical method used by Lekhnitskii [3]. The cost function was regarded as the maximum stress created around the hole and was calculated using the aforementioned analytical approach. The finite element method was then employed to verify the results of the analytical calculation. The overlap in the analytical and FEM calculations confirmed the validity of the solution proposed in this research. The findings further indicated that the design variables significantly affect the stress distribution around quasi-triangular holes and structural load-bearing capacity. The performance of the PSO algorithm was also investigated.

© 2018 Published by Semnan University Press. All rights reserved.

1. Introduction

Composite plates are characterized by superior mechanical properties, such as high strength-to-weight ratios, which is why these materials are increasingly used in building industries and many other important sectors. The wide application of composite plates and their complicated behavioral nature compared with that of metals necessitate a detailed study of their failure strength. The numerous applications of composite plates also generate a variety of geometric discontinuities with different sizes and shapes. Examples of such discontinuities are holes on the doors and windows of submarines and airplanes, points for mounting manometers and barometers on a furnace wall, points of junction between plates and rivets and screws, holes that enable the easy flow of cooling fluids across turbine blades, and holes created to enable the passing of electrical cables and hydraulic hoses or the facilitation of fuel flow on a wing. In all these cases, geometric changes in different structures create highly localized stresses around discontinuous areas, where structural failure usually occurs. Analyzing stress concentration is therefore essential for designers of engineering structures because the fracture strength of these constructions depends strongly on the stress concentration caused by holes. Stress concentration is also critical in evaluating the reliability of engineering structures. The stress surrounding fastened joints, for example, causes 80% of fatigue failures in aircraft structures [1].

2. Literature review

Savin [2] was the first to study an infinite plate containing a triangular hole with rounded edges—a task that he carried out using conformal mapping and the Schwarz relation. The author examined stress concentration around different holes in isotropic plates and around circular and elliptical

* Corresponding author. Tel.: +98-9153213144
E-mail address: m_jafari821@shahroodut.ac.ir
DOI: 10.22075/MACS.2018.1749.1088

holes in anisotropic plates. He also calculated the stress distribution around an equilateral triangular hole with rounded corners in infinite plates. Lekhnitskii [3] explored anisotropic plates containing circular and elliptical holes, while Theocaris and Petro [4] investigated the stress distribution around an equilateral triangular hole and the effects of bluntness. With the expansion of Savin's method, Daoust and Hoa [5] analyzed equilateral triangular holes in infinite isotropic and anisotropic plates subjected to uniaxial loading. Apart from scrutinizing these holes, they investigated other triangular holes with different aspect ratios and the effects of curvature bluntness on the stress distribution around the holes. Tsutsumi et al. [6] explored the solution of a semi-infinite plane with one circular hole. The authors arrived at their solution by repeatedly superposing the solution of an infinite plane with one circular hole and that of a semi-infinite plane without holes to cancel out the stresses arising on both boundaries.

Rezaeepazh and Jafari [7–8] illuminated the stress distribution around several non-circular holes in isotropic and composite plates using Lekhnitskii's [3] solution. Asmar and Jabbour [9] calculated the stress distribution around a rectangular hole in an infinite anisotropic plate under tensile loading. They examined the effects of bluntness and load angle on the stress analysis of perforated plates. On the basis of Savin's [2] potential function, Rao et al. [10] presented relationships for the stress analysis of isotropic and anisotropic plates containing a rectangular hole. Yang et al. [11] used the Airy stress function to look into exact solutions for the stresses, strains, and displacements in a perforated rectangular plate—problems that stem from an arbitrarily located circular hole subjected to both linearly varying in-plane normal stresses on two opposite edges and in-plane shear stresses.

Sivakumara et al. [12] probed into the optimization of laminate composites containing an elliptical hole by using a genetic algorithm. The design variables used by the authors were the stacking sequence of laminates, the thickness of each composite layer, the relative size of a hole, hole orientation, and ellipse diameters. They also regarded first and second natural frequencies as cost functions. Liu et al. [13] presented a newly developed fixed grid evolutionary structural optimization method to obtain the optimum shape of multiple holes in composite structures on the basis of the Tsai–Hill failure criterion. The authors first considered the effects of the number of holes and the spacing relative to each hole, then they used the Tsai–Hill failure criterion for a composite plate to evaluate the cost function. Cho and Rowlands [14] demonstrated the effectiveness of a genetic algorithm in minimizing the tensile stress concentration in composite laminates containing holes. Along with the algorithm, a specially developed finite element program was used by the authors. Hudson et al. [15] employed ant colony optimization for the multiple objective optimization of composite sandwich structures for rail vehicle floor panels. Almeida and Awruch [16] delved into the optimal design of laminate composites using a genetic algorithm and finite element approaches. The authors regarded fiber angle and the thickness of each composite layer as design variables and indicated the cost function as achieving the lowest deflection and weight.

Alonso et al. [17] used particle swarm optimization (PSO) on the basis of moving bird groups to optimized composite structures. Also using PSO and a finite element method (FEM), Chen et al. [18] presented an optimization approach to ensuring the reliability of composite structures. The authors used ANSYS data in MATLAB and presented numerical examples of laminates, composite cylindrical shells, and composite pressure vessels to verify the effectiveness of their method. Sharma et al. [19] optimally designed symmetrical laminate composites containing an elliptical hole by using a genetic algorithm. They obtained the optimum fiber angle in the composites under in-plane loading conditions and calculated the cost function using the Tsai–Hill failure criterion. The design variable that they used was the stacking sequence of laminates. Zhu et al. [20] considered the optimization of composite struts using a genetic algorithm and the Tsai–Hill failure criterion, paying attention to minimizing the weight of a structure and increasing buckling load. The authors adopted fiber volume fraction and the stacking sequence of laminates as design variables. Jafari et al. [21] calculated the optimum values of the effective design variables acting on the stress distribution around different holes by using the genetic algorithm.

In this study, a PSO algorithm was used to determine the optimal values of effective parameters that act on the stress distribution around a quasi-triangular hole in an orthotropic plate. Previous studies minimally investigated the effects of these parameters on the stress distribution around holes. Specifically, the research relied on Lekhnitskii's [3] analytical solution and expanded it for application to the quasi-triangular hole for the purpose of determining the optimal values of the design variables for uniaxial, equi-biaxial, and shear loading and generating the

minimum normalized stress. Because of the traction-free boundary conditions imposed on a hole's edge, stresses σ_ρ and $\tau_{\rho\theta}$ at the hole's edge are zero, and circumferential stress σ_θ is the only remaining stress. In this research, minimizing normalized stress around the hole is considered the cost function. Normalized stress is the ratio of the maximum value of circumferential stress at the edge of the hole (σ_θ) to nominal or applied stress.

3. Particle Swarm Optimization

PSO was presented by Kennedy and Eberhart [22]. In an $N_{var}-$dimensional problem, a particle includes a row vector with N_{var} elements. This arrangement is defined as Eq. (1). To initiate the algorithm, a number of these particles (as the number of the primary particle algorithm) must be created. The total particle matrix is then formed and expressed as Eq. (2).

$$\text{particle} = [p_1, p_2, p_3, \dots, p_{N_{var}}] \quad (1)$$

$$\text{particles} = \begin{bmatrix} \text{particle}_1 \\ \text{particle}_2 \\ \text{particle}_3 \\ \vdots \\ \text{particle}_N \end{bmatrix} = \begin{bmatrix} p_{1,1}, p_{2,1}, \dots, p_{N_{var,1}} \\ p_{1,2}, p_{2,2}, \dots, p_{N_{var,2}} \\ p_{1,3}, p_{2,3}, \dots, p_{N_{var,3}} \\ \cdot \\ \cdot \\ \cdot \\ p_{1,N}, p_{2,N}, \dots, p_{N_{var,N}} \end{bmatrix} \quad (2)$$

As previously stated, the cost function is to minimize normalized stress, which is the ratio of the maximum value of circumferential stress at the edge of the hole (σ_θ) to nominal or applied stress. The cost of each particle is obtained by evaluating the cost function for variables $p_1, p_2, p_3, \dots, p_{N_{var}}$ in accordance with Eq. (3).

$$C.F._i = f(p_1, p_2, p_3, \dots, p_{N_{var}}) \quad (3)$$

In the PSO algorithm, the particles update their velocities and positions on the basis of the best absolute and local solution, as in Eqs. (4) and (5) [23].

$$V_{i,j}(t+1) = \omega V_{i,j}(t) + r_{1,j}.c_1\left(P_{i,j}(t) - X_{i,j}(t)\right) + r_{2,j}.c_2\left(P^*_{i,j}(t) - X_{i,j}(t)\right) \quad (4)$$

$$X_{i,j}(t+1) = X_{i,j}(t) + V_{i,j}(t+1) \quad (5)$$

In the equations above, $V_{i,j}(t)$ and $X_{i,j}(t)$ are the current velocity and position of a particle, respectively. Let $X_i(t) = \{x_{i,1}(t), \dots, x_{i,N_{var}}(t)\}$ be the position of particle *i* in an $N_{var}-$dimensional search space at iteration *t*. The updated velocity and position of the particle are $V_{i,j}(t+1)$ and $X_{i,j}(t+1) = \{x_{i,1}(t+1), \dots, x_{i,N_{var}}(t+1)\}$, respectively. Item ω is the inertia weight coefficient, and c_1 and c_2 denote two positive constants called cognitive and social coefficients, respectively. Items $r_{1,j}$ and $r_{2,j}$ are two random vectors, whose elements are $r_{1,j}, r_{2,j} \in [0,1]$, and $P_{i,j}(t)$ and $P^*_{i,j}(t)$ are the best positions of individual and group experiences, respectively. Finally, each particle is updated on the basis of the best performance of its relationship with condition (6). Moreover, the velocity and position of a particle determined on the basis of the best position among particles are updated according to Eq. (7) [24].

$$\text{if} \quad f(X_{i,j}(t+1)) < f(P_{i,j}(t)) \quad \text{then} \quad P_{i,j}(t+1) = X_{i,j}(t+1) \quad (6)$$

$$\text{if} \quad f(X_{i,j}(t+1)) < f(P^*_{i,j}(t)) \quad \text{then} \quad P^*_{i,j}(t+1) = X_{i,j}(t+1) \quad (7)$$

3.1. Convergence performance

PSO has become very popular because of the simplicity with which it is implemented and its effectiveness in quickly converging to a reasonably good solution. The convergence performance of the algorithm depends on the conditions presented in Eq. (8) [25].

$$r_1.c_1 + r_2.c_2 > 0 \ , \ \frac{r_1.c_1 + r_2.c_2}{2} - \omega < 1 \ , \ \omega < 1 \quad (8)$$

We know that $r_1, r_2 \in [0,1]$. As a result, ensuring the convergence of the PSO algorithm requires expressing the above-mentioned inequalities with innovative parameters as Eq. (9). The upper and lower bounds of design variables are defined as Eq. (10).

$$0 < c_1 + c_2 < 4 \quad , \quad \frac{c_1 + c_2}{2} - 1 < \omega < 1 \quad (9)$$

$$\text{subject to:} \quad \begin{Bmatrix} 0 < \theta_i < 90 \ ; (i = 1,2) \\ 0 < \theta_3 < 180 \\ 0 < w < 0.5 \end{Bmatrix} \quad (10)$$

As reflected in Eqs. (4) and (5), some of the particles may leave the feasible region of a search space. To handle these infeasible solutions, the "absorb technique" is applied. In this technique, invalid particles are moved to the nearest boundary by setting all variables outside the feasible region to their nearest bound (Eq. (11)). The affected velocity components are set to zero (Eq. (2)). In Eqs. (11) and (12), l_j and u_j are the lower and upper bounds of the *j*th component of the search space.

$$x_{i,j}(t+1) = \begin{cases} l_j & \text{if } x_{i,j}(t+1) < l_j \\ u_j & \text{if } x_{i,j}(t+1) > u_j \end{cases} \quad (11)$$

$$v_{i,j}(t+1) = 0 \ \text{if} \ x_{i,j}(t+1) < l_j \ \text{or} \ x_{i,j}(t+1) > u_j \quad (12)$$

4. Effects of algorithm parameters

The values of the effective parameters for the PSO algorithm are listed in Table 1. Changing and optimizing these parameters produce a high-performance algorithm. To illustrate, the effects of the parameters related to the algorithms used in this work were investigated. Note that the results represent boron/epoxy composites and uniaxial tensile loading at $w = 0.1$.

4.1. Effects of c1 and c2 in the PSO algorithm

Fig. 1 illustrates the effects of the number of iterations on the cost function at different values of c_1 and c_2. Table 2 presents the values of the cost function and the optimum design variables at different values of c_1 and c_2.

To emphasize the general search of particles in the search space at the beginning of algorithm operation and local search at the end of operation, c_1 is reduced and c_2 is increased. Correspondingly, the particles are attracted to the best position of the swarm. The parameters are updated as Eqs. (13) and (14) [26].

$$c_{1_{(t+1)}} = \left(c_{1,f} - c_{1,i}\right)\frac{t}{t_{max}} + c_{1,i} \tag{13}$$

$$c_{2_{(t+1)}} = \left(c_{2,f} - c_{2,i}\right)\frac{t}{t_{max}} + c_{2,i} \tag{14}$$

where $c_{1,f}$, $c_{2,f}$, $c_{1,i}$, $c_{2,i}$ are constant, t denotes the number of current repetitions of a particle, and t_{max} represents the maximum number of allowable iterations.

Table 1. Values of effective parameters for the PSO algorithm

PSO parameters
Algorithm parameters:
Population size = 50
Maximum of iteration = 40
Cognitive component $c_{1_{(t+1)}} = \left(c_{1,f} - c_{1,i}\right)\frac{t}{t_{max}} + c_{1,i}$
Social component $c_{2_{(t+1)}} = \left(c_{2,f} - c_{2,i}\right)\frac{t}{t_{max}} + c_{2,i}$
Inertia weight $\omega_{t+1} = (\omega_i - \omega_f)\left(\frac{t_{max}-t}{t_{max}}\right) + \omega_f$
$0 < c_1 + c_2 < 4$, $\frac{c_1 + c_2}{2} - 1 < \omega < 1$
Constraints:
Load angle $0 < \theta_1 < 90$
Fiber angle $0 < \theta_2 < 90$
Rotation angle $0 < \theta_3 < 180$
Bluntness factor $0 \le w < 0.5$
Cost Function:
Minimizing normalized stress around the quasi-triangular hole

4.2. Effects of ω in the PSO algorithm

The inertia weight coefficient (ω) directly affects the convergence rate of PSO. This coefficient can be used to control the effects of previous velocities on current velocities, and its value can be modified to improve balance between global and local searches. Shi and Eberhart [22] stated that the optimum value of ω can be improved for most problems by changing the weight coefficient from 0.9 at the beginning of a search to 0.4 at the end of the search.

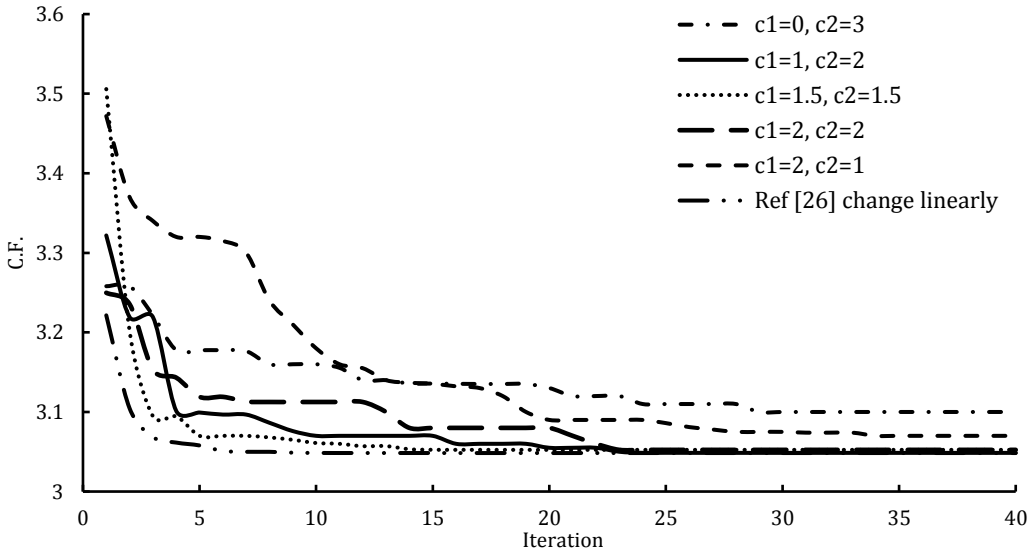

Figure 1. Convergence of cost function at different c_1, c_2 values

Table 2. Optimal values and corresponding cost function at different c_1, c_2 values

	Population size	Number of iterations	θ_1	θ_2	θ_3	C.F.
$c_1 = 0, c_2 = 3$	50	26	8.81	75.3	180	3.1102
$c_1 = 1, c_2 = 2$	50	23	15.85	83.41	8.31	3.0486
$c_1 = 1.5, c_2 = 1.5$	50	24	67.56	0	134.98	3.0523
$c_1 = 2, c_2 = 1$	50	33	79.72	11.07	87.34	3.0793
$c_1 = 2, c_2 = 2$	50	24	67.58	0	52.48	3.0487
Ref. [26]	50	17	4.30	71.76	176.76	3.0484

Fig. 2 depicts the effects of the number of iterations on the cost function at different methods of calculating ω. Table 3 presents the values of the cost function and the optimum parameters under different methods of calculating ω. In the first approach using [26], inertia weight is defined as follows (linearly varying):

$$\omega_{t+1} = (\omega_i - \omega_f)\left(\frac{t_{max} - t}{t_{max}}\right) + \omega_f \quad (15)$$

in which ω_i and ω_f are the primary and final values of inertia weight, respectively. In the second approach (Convergence factor), a PSO algorithm with a convergence factor was defined in [24], and the following formula is used to update the position and speed of particles:

$$V_{i,j}(t+1) = \chi\left\{V_{i,j}(t) + r_{1,j}.c_1\left(P_{i,j}(t) - X_{i,j}(t)\right) + r_{2,j}.c_2\left(P^*_{i,j}(t) - X_{i,j}(t)\right)\right\}$$
$$\chi = \frac{k}{\text{abs}\left(\frac{1-\frac{c}{2}-\sqrt{\text{abs}(c^2-4c)}}{2}\right)} \quad (16)$$

where $k \in [0,1]$, $c = c_1 + c_2$ (c should be smaller than 4.). The third approach enables a dynamic decrease in the inertia weight value if a swarm does not improve the solution after a certain number of iterations [25]. An update is implemented from an initial weight (ω_0) value based on a fraction multiplier $k_\omega \in [0,1]$; that is,

$$\omega_{t+1} = k_\omega.\omega_t \quad (17)$$

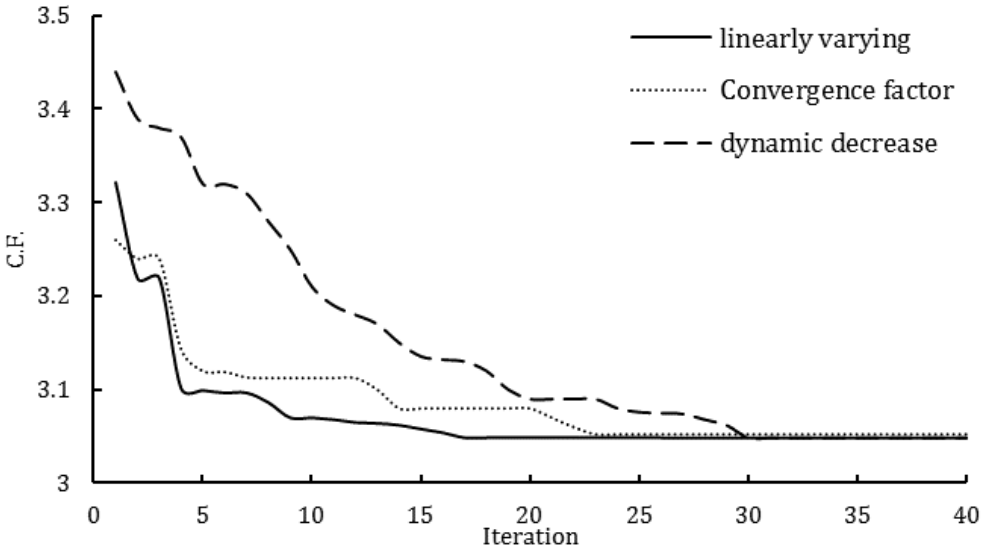

Figure 2. Convergence of the cost function at different approaches to ω

Table 3. Optimal values and corresponding cost function for different approaches to ω

	Population size	Number of iterations	θ_1	θ_2	θ_3	C.F.
Linearly varying	50	16	90	22.42	157.5	3.0484
Convergence factor	50	26	75.15	7.59	82.70	3.0484
Dynamic decrease	50 (k_ω = 0.975)	31	19.38	86.94	11.83	3.0484

5. Problem description

The problem disentangled in this study is an infinite plate containing a quasi-triangular hole. As shown in Fig. 3, the plate is subjected to biaxial loading at angle θ_1 (load angle) with respect to the x-axis. A triangular hole has arbitrary orientations such that its major axis is directed at angle θ_3 (rotation angle) with respect to the x-axis. The fiber angle is θ_2.

Replacing stress–strain relations in a compatibility relation and rewriting the resultant equation in terms of the stress function yield [3]

$$R_{11}\frac{\partial^4 F}{\partial y^4} - 2R_{16}\frac{\partial^4 F}{\partial x\,\partial y^3} + (2R_{12}+R_{66})\frac{\partial^4 F}{\partial x^2\,\partial y^2} - 2R_{26}\frac{\partial^4 F}{\partial x^3\,\partial y} + R_{22}\frac{\partial^4 F}{\partial x^4} = 0 \quad (18)$$

Eq. (18) is the compatibility equation for anisotropic materials, where R_{ij} represents the compliance coefficients of perforated plates. The general solution of this equation depends on the roots of the following characteristic equation:

$$R_{11}S^4 - 2R_{16}S^3 + (2R_{12}+R_{66})S^2 + 2R_{26}S + R_{22} = 0 \quad (19)$$

In general, Eq. (19) can be proved as having four conjugate roots, after which the general expression of the stress function can be indicated thus:

$$F(x,y) = 2\mathrm{Re}[\varphi(z_1) + \psi(z_2)] \quad (20)$$

The equation $z_k = x + S_k y\ (k = 1,2)$ and S_k are the roots of the characteristic equation of anisotropic materials. Finally, stress components in terms of two potential functions of $\varphi(z_1)$ and $\psi(z_2)$ are expressed according to Eq. (21) [7].

$$\begin{aligned}\sigma_x &= \sigma_x^{\infty} + 2\mathrm{Re}\left[{S_1}^2\varphi''(z_1) + {S_2}^2\psi''(z_2)\right]\\ \sigma_y &= \sigma_y^{\infty} + 2\mathrm{Re}\left[\varphi''(z_1) + {S_2}^2\psi''(z_2)\right]\\ \tau_{xy} &= \tau_{xy}^{\infty} - 2\mathrm{Re}[S_1\varphi''(z_1) + S_2\psi''(z_2)]\end{aligned} \quad (21)$$

where

$$\begin{aligned}\sigma_x^{\infty} &= \frac{\sigma}{2}[(\lambda+1) + (\lambda-1)\cos 2\theta_1]\\ \sigma_y^{\infty} &= \frac{\sigma}{2}[(\lambda+1) - (\lambda-1)\cos 2\theta_1]\\ \tau_{xy}^{\infty} &= \frac{\sigma}{2}[(\lambda-1)\sin 2\theta_1]\end{aligned} \quad (22)$$

In Eq. (22), adopting appropriate values of λ and θ_1 for stress applied at infinity $\left(\sigma_x^{\infty}, \sigma_y^{\infty}, \tau_{xy}^{\infty}\right)$ enables the consideration of uniaxial loading, equi-biaxial loading, and shear loading. The following values of λ and θ_1 may be incorporated into Eqs. (22) to obtain various cases of in-plane loading:

Inclined uniaxial tension: $\lambda = 0, \theta_1 \neq 0$

Equi − biaxial tension: $\lambda = 1, \theta_1 = 0$

Shear loading: $\lambda = -1, \theta_1 = {}^{\pi}/_{4}, {}^{3\pi}/_{4}$

Items $\varphi''(z_1)$ and $\psi''(z_2)$ are the derivatives of functions $\varphi(z_1)$ and $\psi(z_2)$ with respect to z_1 and z_2. These analytic functions can be determined by applying boundary conditions.

Eqs. (23) and (24) are used to calculate stress components in the polar coordinate system. In these equations, Ω is the angle between the positive x-axis and ρ (Fig. 4).

$$\sigma_\theta + \sigma_\rho = \sigma_y + \sigma_x \quad (23)$$

$$\sigma_\theta - \sigma_\rho + 2i\tau_{\rho\theta} = (\sigma_y - \sigma_x + 2i\tau_{xy})e^{2i\Omega} \quad (24)$$

As shown in Fig. 5, the infinite orthotropic plate with an arbitrary hole subjected to in-plane loading was examined. No external forces are acting on the hole's edge. The superposition method was used to calculate the stress distribution around the hole. For the no-hole plate subjected to in-plane loading, stress functions $\varphi_1(z_1)$ and $\psi_1(z_2)$ were calculated (Fig. 5a).

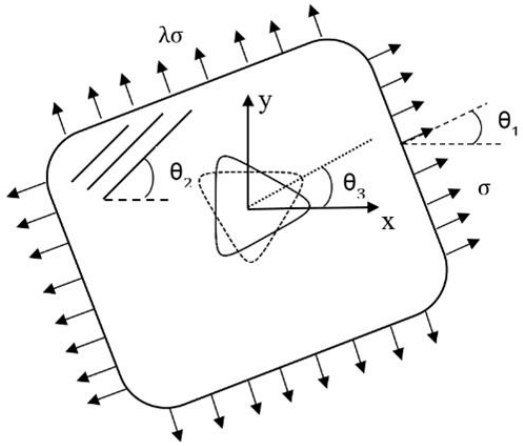

Figure 3. Perforated orthotropic plate subjected to biaxial loading

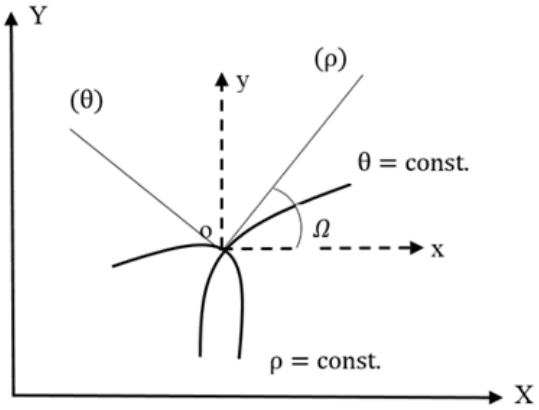

Figure 4. Curvilinear coordinates

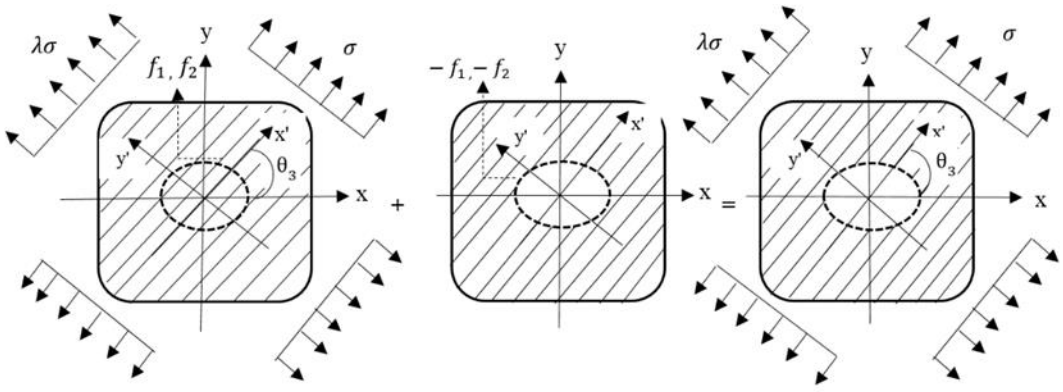

Figure 5. Scheme for the superposition of a solution for a perforated plate under biaxial loading; (a) plate without a hole, loading at infinity; (b) plate with negative loading on the edge of the hole; (c) plate with an arbitrary hole, loading at infinity [27]

In this stage, using the aforementioned stress functions enabled the calculation of the boundary conditions (f_1 and f_2) located on the edge of a fictitious hole. Then, the plate with a hole and subjected to negative distributed loads $-f_1$ and $-f_2$ at the hole's edge was analyzed (Fig. 5b). In this case, stress functions $\varphi_0(z_1)$ and $\psi_0(z_2)$ were obtained on the basis of the Ukadgaonker solution [27].

The stress functions for a perforated plate with a traction-free hole and loading at infinity are obtained via the superposition of the stress functions in the stages discussed above; that is,

$$\varphi(z_1) = \varphi_1(z_1) + \varphi_0(z_1) \quad (25)$$
$$\psi(z_2) = \psi_1(z_2) + \psi_0(z_2) \quad (26)$$

Finally, stress components are obtained by replacing the stress functions in Eq. (21) with the above-mentioned stress functions.

5.1. Conformal mapping

With the analytical solution proposed by Lekhnitskii [3], the stress distribution around a circular or an elliptical hole in anisotropic plates was obtained. To use this method as a means of examining plates with triangular holes, an essential requirement is to apply the mapping function, similar to what is presented in Eq. (27). According to this conformal mapping, the infinite area external to a hole can be transformed by the area outside a unit circle.

$$Z = x + s_k y \quad (27)$$

where

$$x = \cos\theta + w\cos(2\theta)$$
$$y = -(\sin\theta - w\sin(2\theta)) \quad (28)$$

In the relation above, parameter w determines the bluntness factor and changes the radius of curvature at the corner of the hole. Changing the value of w from zero to 0.3 reduces the curvature of the corners of the triangular hole (Fig. 6). As can be concluded from Eq. (28), $w = 0$ represents a circular hole. Bluntness (w) and hole orientation (θ_3) are important design variables that influence the stress distribution around different holes.

6. Verification of results

FEM (ABAQUS) was used to verify the accuracy of the analytical results. First, for the orthotropic plate with a quasi-triangular hole (w = 0.15), the optimum values were obtained using the optimization code written in MATLAB. Second, considering the optimum values of the effective design variables (θ_1 = 90°, θ_3 = 30°, θ_2 = 22°) enabled the modeling of the problem described in the previous section in ABAQUS. Mesh sensitivity was scrutinized, and an acceptable mesh was chosen. Fig. 7 shows the comparison of the stress distributions obtained via the analytical solution and FEM for a glass/epoxy composite.

Fig. 8 shows the comparison of the results obtained via the analytical method and FEM for a boron/epoxy composite; the comparison involved considering the optimum values calculated through the PSO optimization code written in MATLAB (θ_1 = 90°, θ_3 = 157°, θ_2 = 20.40°). The findings derived via the analytical solution and FEM exhibit good agreement, indicating the accuracy and precision of the proposed analytical solution.

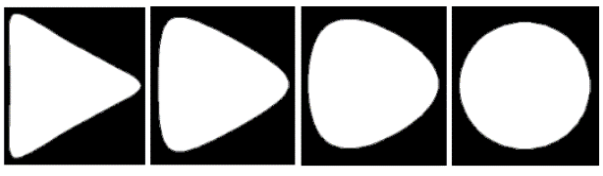

Figure 6. Effects of w on the shape of the quasi-triangular hole

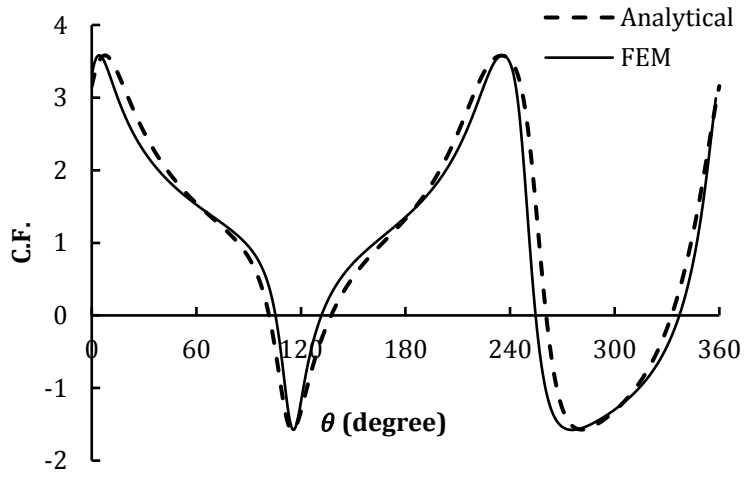

Figure 7. Comparison of the FEM and analytical results for glass/epoxy composites (w = 0.15)

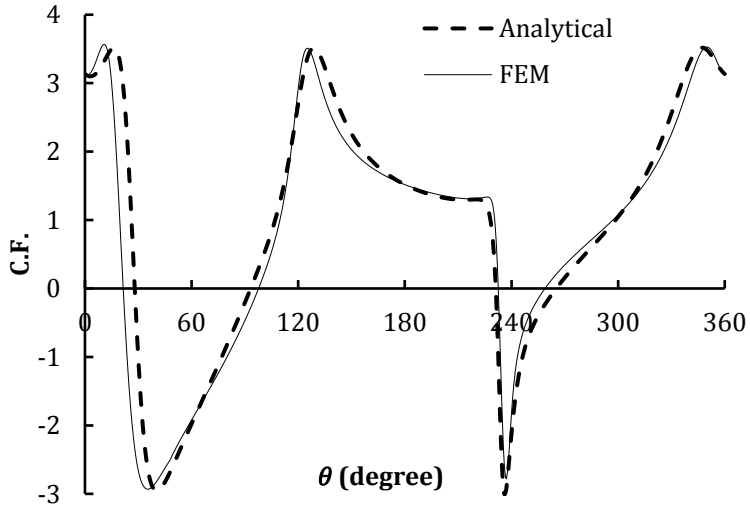

Figure 8. Comparison of FEM and analytical results for boron/epoxy (w = 0.15)

7. Results

As mentioned earlier, this research ascertained the optimal values of design variables that affect the stress distribution around a quasi-triangular hole in an infinite orthotropic plate by using PSO. To achieve this aim, for uniaxial loading and determining the specific value of each design variable, the optimum values of other design variables and their corresponding cost function were determined. Then, taking into account all the design variables, the value of the cost function was incorporated into various cases of in-plane loading. The mechanical properties of the materials examined are presented in Table 4. The effects of hole orientation on the value of the cost function at a range of load angles (uniaxial loading), at a w = 0.05, and for a glass/epoxy composite are shown in Fig. 9. These results are presented in the optimum fiber angles obtained using the PSO algorithm. As indicated in the figure, at different load angles, the value of the cost function varies with hole orientation. These variations with rotation angle occurs at 60°. Although these results are applicable only to glass/epoxy composites, such periodic behavior can also be observed in other materials. Fig. 10 presents the effects of fiber angle on the value of the cost function at different load angles for a glass/epoxy composite. These findings are presented in the optimum hole orientation obtained using the PSO algorithm. As the figure reflects, the maximum and minimum values of the cost function at different load angles occur identically at different fiber angles.

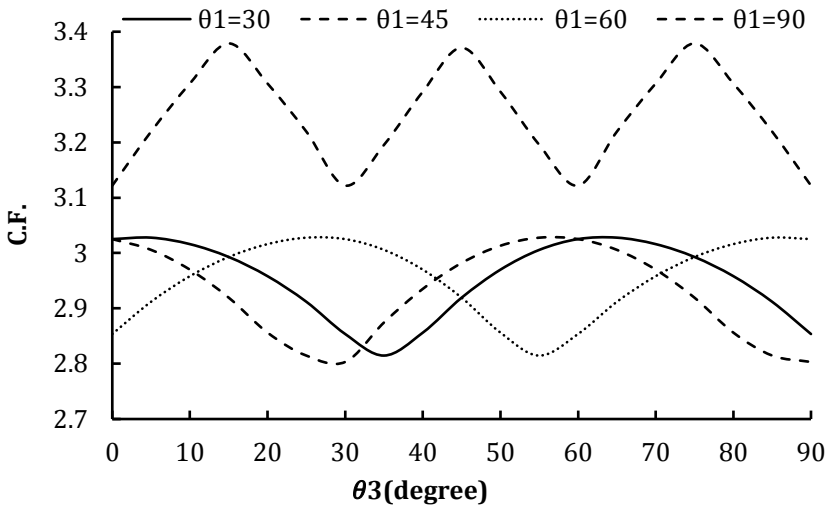

Figure 9. Variations in the cost function with respect to hole orientation at an optimum fiber angle (glass/epoxy)

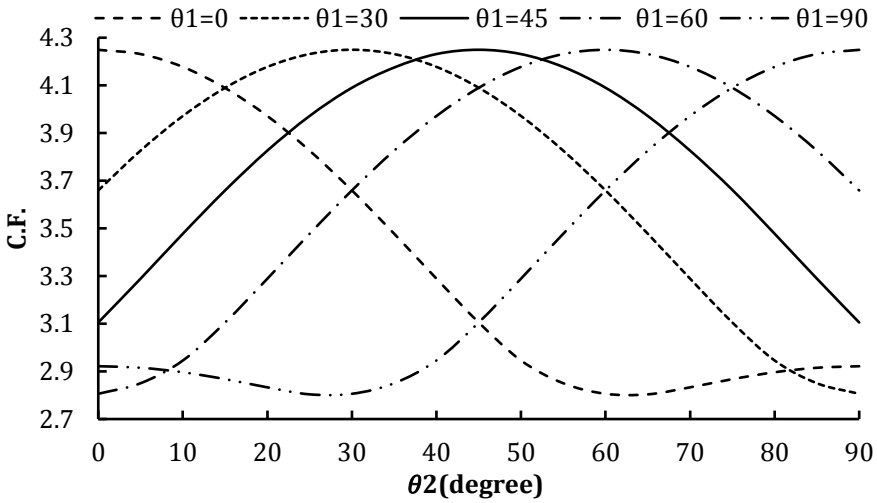

Figure 10. Variation of the cost function with respect to fiber angle in different load angles (Glass/Epoxy)

Table 4. Properties of the plates

	E_1 (GPa)	E_2 (GPa)	G_{12} (GPa)	ν_{12}
Graphite/epoxy (T300/5208)	181	10.3	7.17	0.28
Carbon/epoxy (IM6/SC1081)	177	10.8	7.6	0.27
Boron/epoxy(B5.6/5505)	201	21.7	5.4	0.17
Glass/epoxy	38.6	8.27	4.14	0.26

Fig. 11 shows the effect of hole orientation on the cost function at different values of bluntness factor. These results are applicable to the optimum fiber angle and $\theta_1 = 0$. As expected, a decreasing w and hole softening reduce the value of the cost function. The minimum value of the cost function occurs at w = 0, which is equivalent to a circular hole.

Table 5 lists the optimum values provided in Figs. 9 to 11. We endeavored to present the results for glass/epoxy (uniaxial loading) composites in detail, but for other materials, only the optimum values of design variables are provided.

Fig. 12 shows the variations in the cost function with respect to fiber angle at various rotation angles. In this case, the design variable used was load angle, which was determined using the PSO algorithm. Fig. 13 shows the variations at different values of bluntness factor and $\theta_3 = 0$. Fiber angle was considered a design variable. As shown in the figure, except for the circular hole (w = 0), the maximum value of the cost function occurs at a load angle close to 50°. A load angle of 0° leads to the lowest possible value of the cost function.

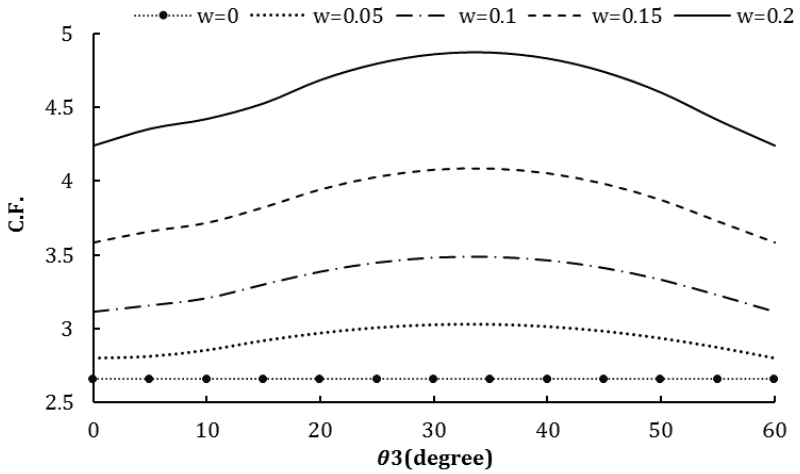

Figure 11. Effects of rotation angle on the cost function at different bluntness values, optimum fiber angle, and θ_1=0 (glass/epoxy)

Table 5. Optimum hole orientation and fiber angle at various load angles and bluntness values (glass/epoxy)

	θ_1	θ_2	θ_3	C.F.		θ_1	θ_2	θ_3	C.F.
	0	59.4	-	2.6595		0	68.80	0	3.5821
	30	89.3	-	2.6595		30	90	35.5	3.6647
	45	90	-	2.6595		45	0	31	3.9289
w = 0	60	0.6	-	2.6595	w = 0.15		90	59	
	90	30.5	-	2.6595		60	0	54.5	3.6638
						90	22	30	3.5790
	0	62.7	179	2.8060		0	68.38	60	4.2410
	30	90	153.5	2.8060		30	90	36.34	4.3770
	45	0	150	3.1051		45	0	29.75	4.6606
w = 0.05		90	180		w = 0.2		90	0	4.6643
	60	0	176.5	2.8060		60	0	53.64	4.3791
	90	27.5	149	2.8060		90	19.96	30.69	4.2304
	0	66.3	179.8	3.1147					
	30	90	155	3.1540					
	45	0	151	3.4226					
w = 0.1		90	180						
	60	0	175.45	3.1537					
	90	24	149.8	3.1145					

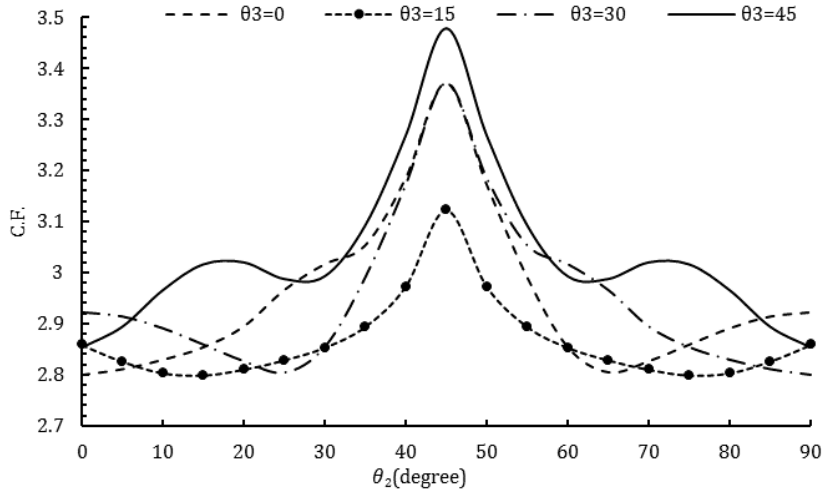

Figure 12. Variations in the cost function in terms of fibers angle at an optimum load angle (glass/epoxy, w = 0.05)

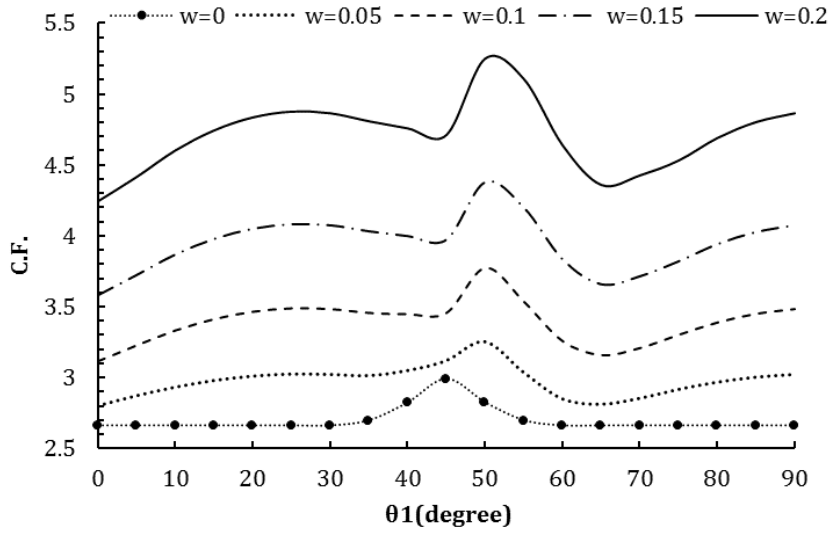

Figure 13. Effects of load angle on the cost function at an optimum fiber angle and different bluntness values (glass/epoxy, θ_3=0)

Table 6 presents the optimum values of load and fiber angles at different hole orientations. Note that at w = 0 during various runs of the program, the minimum value of the cost function occurs at different load and fiber angles; in all runs, the absolute difference between load and fiber angles is 60°.

Table 6. Optimum load and fiber angles at different hole orientations (glass/epoxy, w = 0.05)

	$\theta_3 = 0$				$\theta_3 = 15$			
	θ_2	θ_1	$\lvert\theta_1 - \theta_2\rvert$	C.F.	θ_2	θ_1	$\lvert\theta_1 - \theta_2\rvert$	C.F.
w = 0	90.12	29.78	60.34	2.6595	90	30.77	59.23	2.6595
	59.37	0	59.37	2.6594	30.81	90	59.19	2.6595
	59.38	76.96	59.38	2.6595	12.90	72.35	59.45	2.6595
	0	59.52	59.52	2.6595	9.65	69.03	59.38	2.6595
w = 0.05	0	61.8	61.80	2.7991	76.54	13.85	62.69	2.7982
	64.85	0	64.85	2.7991	13.75	76.27	62.52	2.7982
w = 0.1	0	62.40	62.40	3.1313	80.96	14.89	66.07	3.1147
	66.31	0	66.31	3.1313	12.27	76.22	63.95	3.1209
w = 0.15	68.83	0.37	68.46	3.5788	5.52	74.49	68.97	3.5789
	67.45	0	67.45	3.5812	83.83	15.37	68.46	3.5788
w = 0.2	0	63.35	63.35	4.3214	3.86	74.30	70.44	4.2341
	90	0	90	4.3216	90	16.12	73.88	4.2397
	$\theta_3 = 30$				$\theta_3 = 45$			
	θ_2	θ_1	$\lvert\theta_1 - \theta_2\rvert$	C.F.	θ_2	θ_1	$\lvert\theta_1 - \theta_2\rvert$	C.F.
w = 0	82.48	23.11	59.37	2.6595	14.46	73.83	59.37	2.6595
	22.38	81.75	59.37	2.6595	22.48	81.86	59.38	2.6595
	63	3.63	59.37	2.6595	68.64	9.46	59.18	2.6595
	10.83	70.23	59.40	2.6595	23.54	82.95	59.41	2.6595
w = 0.05	25.10	90	64.90	2.8031	0	54.75	54.75	2.8532
	90	28.20	61.80	2.8031	90	35.25	54.75	2.8532
w = 0.1	23.68	90	66.32	3.1145	0	54.76	54.76	3.2051
	90	27.60	62.40	3.1316	90	35.23	54.77	3.2048
w = 0.15	0	90	90	3.6558	90	34.98	55.02	3.7148
	20.73	89.53	68.8	3.5789	0	55.01	55.01	3.7150
w = 0.2	18.86	89.30	70.44	4.2311	90	34.62	55.38	4.2772
	21.57	90	68.43	4.2400	86.21	33.06	53.15	4.4388
	90	26.64	63.36	4.3219	0	55.36	55.36	4.4262

Fig. 14 shows the variations in the cost function with bluntness factor *w* (uniaxial tensile loading) for different materials. In this case, the values of other design variables (θ_1, θ_2, θ_3) are their optimum values obtained via the PSO algorithm.

According to the figure, for all the materials, a decreasing *w* reduces the value of the cost function. For *w* = 0, the value of the cost function is the lowest possible value. Fig. 15 indicates the stress distribution at different values of *w* and different materials under optimal situations.

Figs. 16 and 17 display the changes in the normalized stress (cost function) around a triangular hole in optimal conditions for glass/epoxy and boron/epoxy composites at three values of *w*, respectively.

Finally, Table 7 presents the optimum values of different design variables, such as load angle, fiber angle, and hole orientation, which were obtained through PSO for different *w* values, all the materials, and various cases of loading, such as equi-biaxial loading, uniaxial tensile loading, and shear loading.

Figs. 18 and Fig. 19 show the changes in the normalized stress around a triangular hole in optimal conditions for glass/epoxy and boron/epoxy composites under equi-biaxial and shear loading and *w* = 0.1.

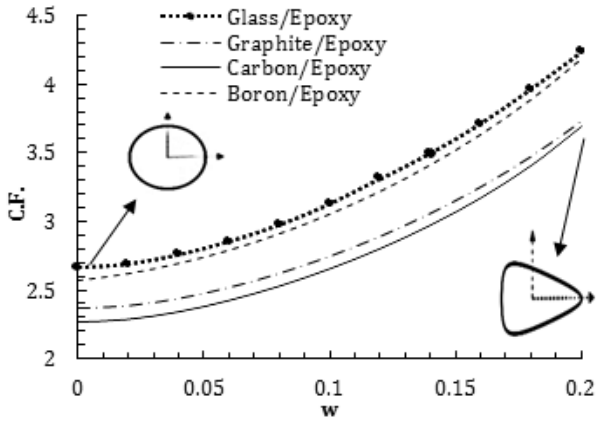

Figure 14. Effects of bluntness on the cost function for different materials

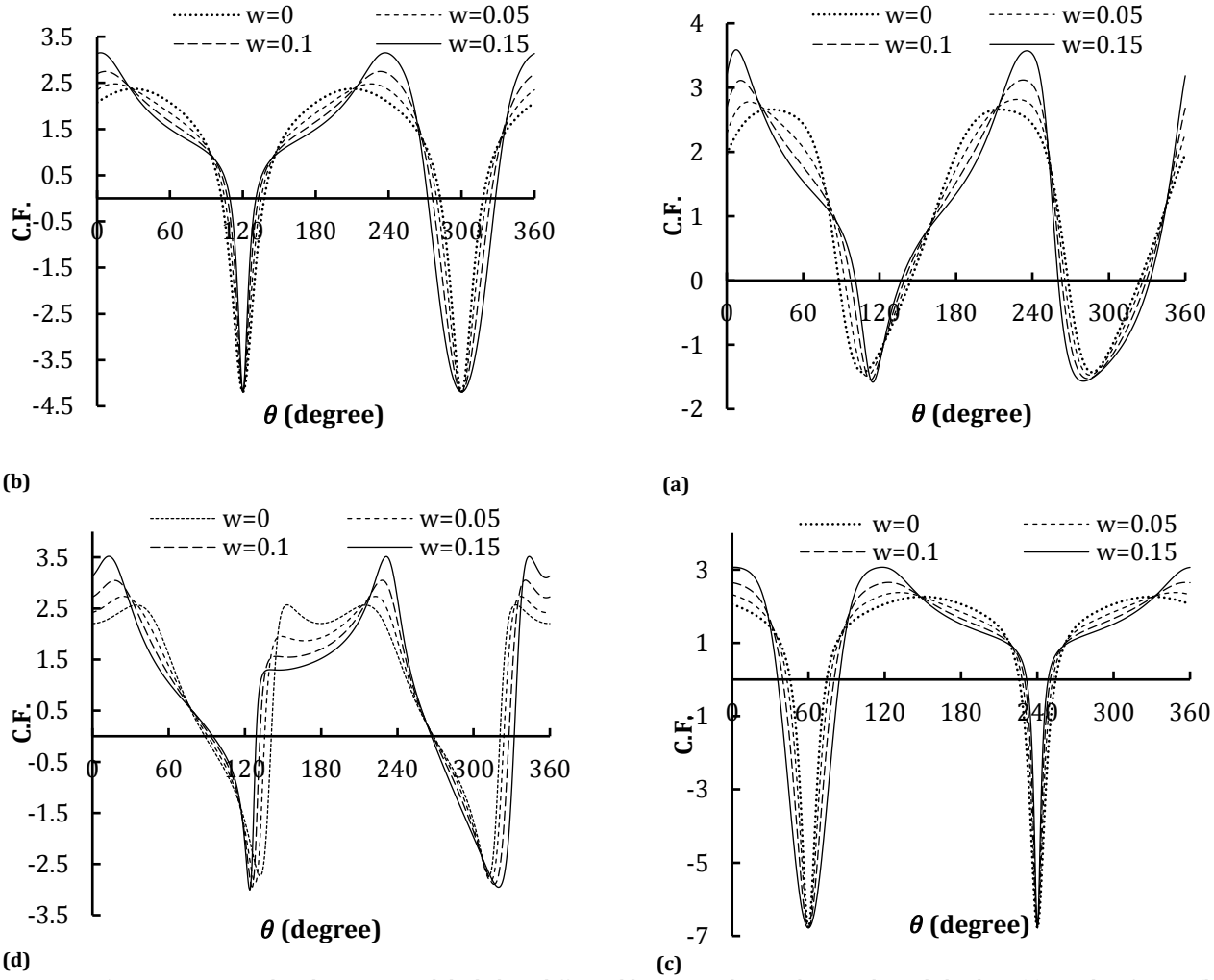

Figure 15. Optimum stress distribution around the hole at different bluntness values and uniaxial tensile loading. (a) Graphite/epoxy, (b) glass/epoxy, (c) boron/epoxy, (d) carbon/epoxy

8. Conclusion

This research inquired into the optimum values of effective design variables for the stress analysis of an infinite orthotropic plate with a quasi-triangular hole. The plate was subjected to uniaxial, equi-biaxial, and shear loading, and the PSO algorithm was used to calculate the optimum values of design variables. As the design variables, bluntness, hole orientation, fiber angle, and load angle are the most important design variables that influence the stress distribution around triangular holes. The optimum values of these design variables were determined for different materials, minimizing normalized stress around the hole was considered the cost function. The results showed that the curvature radius of the hole's corners is not the only parameter that effectively reduces normalized stress and that the appropriate selection of other effective design variables, such as fiber angle, load angle, and hole orientation, significantly reduces normalized stress.

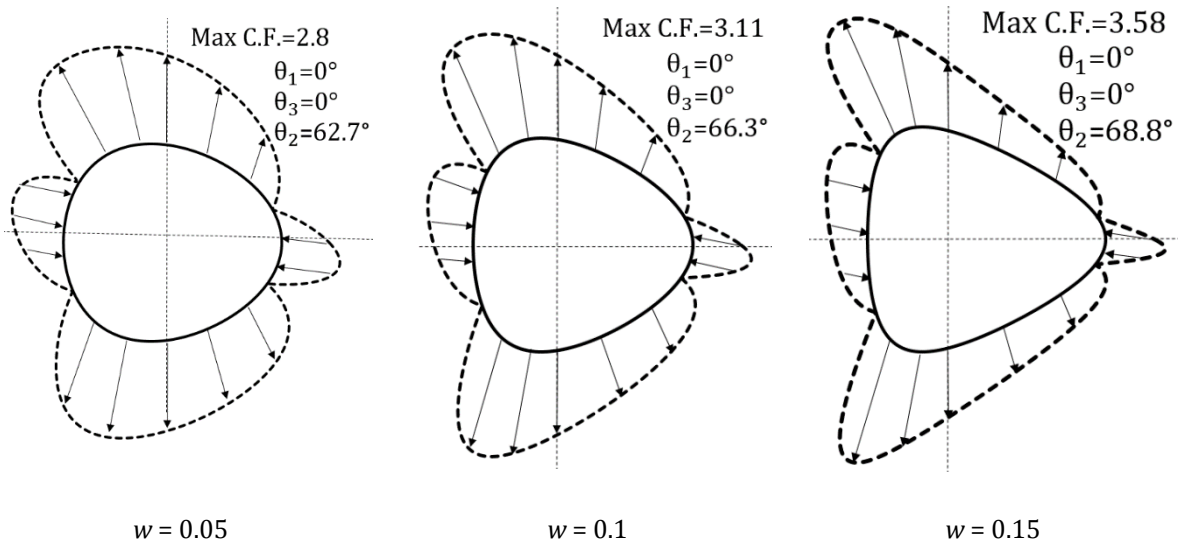

Figure 16. Stress distribution around the hole at different bluntness factors and optimum conditions (glass/epoxy)

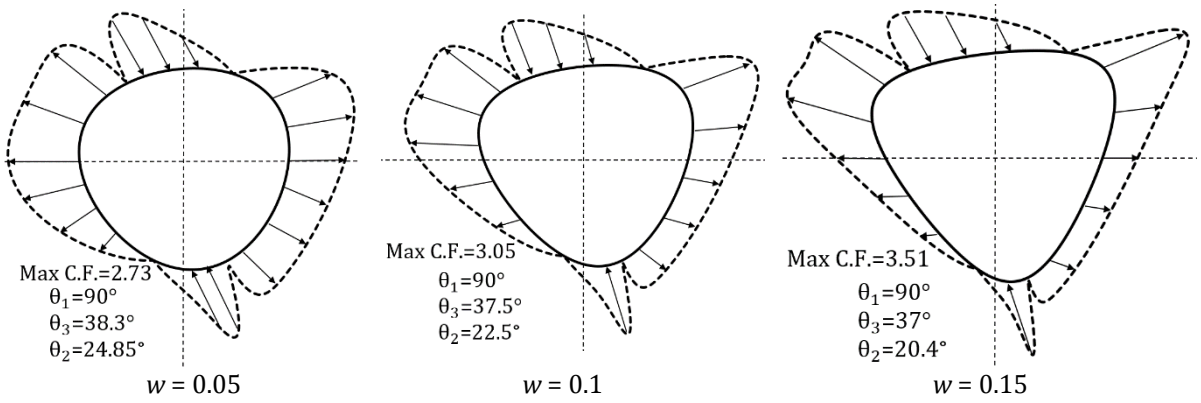

Figure 17. Stress distribution around the hole at different bluntness factors and optimum conditions (boron/epoxy)

Table 7. Optimum values of design variables at different bluntness factors and different loading cases

CE9000 Glass/Epoxy

	Equi-biaxial loading			Uniaxial tensile loading				Shear loading		
w	θ_2	θ_3	C.F.	θ_1	θ_2	θ_3	C.F.	θ_2	θ_3	C.F.
0*	60.79	147.79	2.3977	0	59.4	-	2.6595	0	-	4.1183
	9.17	12.17	2.3977	90	30.5	-	2.6595	90	-	4.1183
	25.86	116.86	2.3977							
0.05	60	180	2.6830	0	62.7	180-120-60-0	2.7982	0	25.7-85.70-145.71	4.2002
	87.02	27.05	2.6832	90	27.5	150-90-30	2.7981	90	4.28-64.28-124.28	4.2005
0.1	0	180	3.3104	0	66.3	180-120-60-0	3.1140	0	25.35-85.37-145.32	4.4421
	90	90	3.3104	90	24	150-90-30	3.1146	90	4.64-64.62-124.64	4.4427
0.15	0	180	4.1786	0	68.8	180-120-60-0	3.5780	0	24.87-84.87-144.87	4.8536
				90	22	150-90-30	3.5780	90	5.14-65.16-125.12	4.8534

Boron/Epoxy

	Equi-biaxial loading			Uniaxial tensile loading				Shear loading		
w	θ_2	θ_3	C.F.	θ_1	θ_2	θ_3	C.F.	θ_2	θ_3	C.F.
0*	63.62	140.62	4.1763	0	62	-	2.5651	0	0.92-60.93-120.93	6.0202
	6.24	51.24	4.1763	90	28	-	2.5651	90	12.60-72.60-132.60	6.0420
	50.30	75.30	4.1765							
0.05	0	180	4.5222	0	65.1	171.7-111.7-	2.7341	0	26.66-86.66-146.68	6.1427
				90	24.8	51.7	2.7341	90	3.15-63.33-123.35	6.2498
0.1	0	180	5.5161	0	67.5	158.3-98.3-	3.0482	0	28.10-88.15-148.12	6.5127
				90	22.5	38.3	3.0482	90	1.44-61.45-121.45	6.5278
0.15	40.41	100.97	7.0087	0	69.6	172.5-112.5-	3.5153	0	28.96-88.96-148.96	6.9324
	20.40	19.85	7.0087	90	20.4	52.5	3.5153	90	1.03-61.06-121.06	6.9315
	0	0	7.0135			157.5-97.5-				
						37.5				
						173-113-53				
						157-97-37				

GY-70/934 Carbon/Epoxy

	Equi-biaxial loading			Uniaxial tensile loading				Shear loading		
w	θ_2	θ_3	C.F.	θ_1	θ_2	θ_3	C.F.	θ_2	θ_3	C.F.
0*	65.17	112.17	2.7523	90	0	-	2.2610	0	8.55-68.55-128.55	9.0581
	85.95	132.95	2.7524	0	90	-	2.2610	90	43.44-103.44-	9.0581
	81.50	40.50	2.7524						163.44	
0.05	0	180	3.5654	0	90	180-120-60-0	2.3744	0		9.2684
				90	0	150-90-30	2.3744	90	21.14-81.14-141.14	9.2684
0.1	0	180	5.1959	0	90	180-120-60-0	2.650	0	8085-68.83-128.83	9.7425
				90	0	150-90-30	2.6500	90	22.67-82.64-142.68	9.7423
0.15	0	180	7.3399	0	90	180-120-60-0	3.0650	0	7.32-67.35-127.36	10.7697
				90	0	150-90-30	3.0650	90	23.23-83.31-143.24	10.7699
									6.76-66.76-126.72	

Graphite/Epoxy(T300/5208)

	Equi-biaxial loading			Uniaxial tensile loading				Shear loading		
w	θ_2	θ_3	C.F.	θ_1	θ_2	θ_3	C.F.	θ_2	θ_3	C.F.
0*	3.80	20.80	2.5515	0	90	-	2.3711	0	10.83-80.82-130.83	6.4761
	64.18	65.18	2.5515	90	0	-	2.3711	90	51.16-111.16-	6.4763
	13.49	88.49	2.5518						171.16	
0.05	0	0	3.1173	0	90	180-120-60-0	2.4770	0		6.6148
				90	0	150-90-3	2.4770	90	25.05-85.05-145.05	6.6145
0.1	0	0	4.2163	0	90	180-120-60-0	2.7473	0	64.94-124.94	7.0071
				90	0	150-90-30	2.7473	90	24.82-84.82-144.82	7.0071
0.15	0	180	5.7482	0	90	180-120-60-0	3.1525	0	5.17-65.17-125.17	7.6716
				90	0	150-90-30	3.1525	90	25.75-85.75-145.75	7.6712
									4.24-64.24-124.24	

* Optimum value

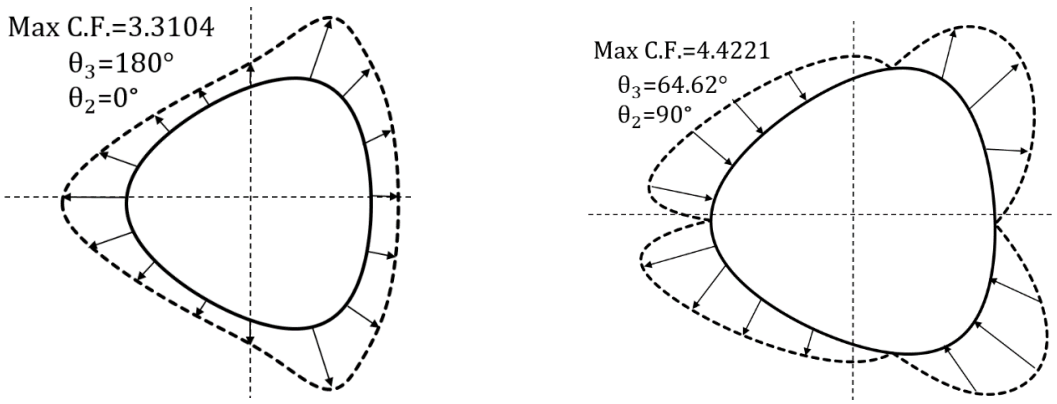

(a) (b)

Figure 18. Stress distribution around the hole under optimum conditions and w = 0.1 for glass/epoxy composites; (a) equi-biaxial loading, (b) shear loading

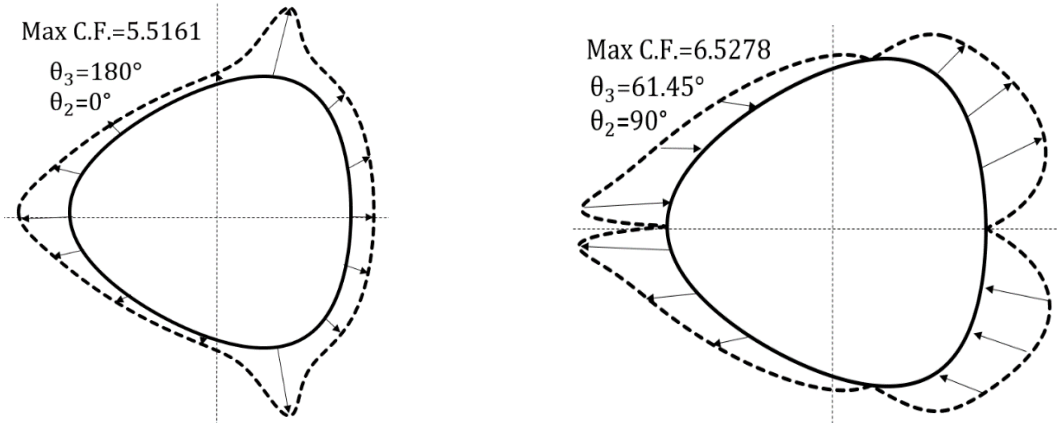

(a) (b)

Figure 19. Stress distribution around the hole under optimum conditions and w = 0.1 for boron/epoxy composites; (a) equi-biaxial loading, (b) shear loading

References

[1] Gao CY, Xiao JZ, Ke YL. FE Analysis of Stress Concentrations in Composite Plates with Multiple Holes for Zigzag Multi-Fastened Joints. *Mater Sci Forum* 2013;770:17–20.

[2] Savin G. Stress Distribution Around Holes, *New York, Pergamon Press* 1961.

[3] Lekhnitskii SG. Anisotropic Plates. *New York, Gordon and Breach Science Publishers* 1968.

[4] Theocaris PS, Petrou L. Stress Distributions and Intensities at Corners of Equilateral Triangular Holes. *Int J Fract* 1986;31:271–289.

[5] Daoust J, Hoa SV. An Analytical Solution for Anisotropic Plates Containing Triangular Holes. *Compos Struct* 1991;19:107–130..

[6] Tsutsumi T, Sato K, Hirashima KI, Arai H. Stress Fields on an Isotropic Semi-infinite Plane with a Circular Hole Subjected to Arbitrary Loads Using the Constraint-Release Technique. *Steel Compos Struct* 2002;2:237–246.

[7] Rezaeepazhand J, Jafari M. Stress Analysis of Perforated Composite Plates. *Compos Struct* 2005;71:463–468.

[8] Rezaeepazhand J, Jafari M. Stress Concentration in Metallic Plates with Special Shaped Hole. *Int J Mech Sci* 2010;52:96–102.

[9] Asmar TJ. Stress Analysis of Anisotropic Plates Containing Rectangular Holes. *Int J Mech Solids* 2007;2:55–84.

[10] Nageswara RDK, Ramesh BM, Raja NRK, Sunil D. Stress Around Square and Rectangular Holes in Symmetric Laminates. *Compos Struct* 2010;92:2845–2859.

[11] Yang YB, Kang JH. Exact Deformation of an Infinite Rectangular Plate with an Arbitrarily Located Circular Hole Under In-plane Loadings. *Struct Eng Mech* 2016;58:783–797.

[12] Sivakumar K, Iyengar NGR, Deb K. Optimum Design of Laminated Composite Plates with Holes Using a Genetic Algorithm. *Compos Struct* 1998;42:265–279.

[13] Liu Y, Jin F, Li Q. A Strength-Based Multiple Hole Optimization in Composite Plates Using Fixed Grid Finite Element Method. *Compos Struct* 2006;73:403–412.
[14] Cho HK, Rowlands RE. Reducing Tensile Stress Concentration in Perforated Hybrid Laminate by Genetic Algorithm. *Compos Sci Technol* 2007;67:2877–2883.
[15] Hudson CW, Carruthers JJ, Robinson AM. Multiple Objective Optimisation of Composite Sandwich Structures for Rail Vehicle Floor Panels. *Compos Struct* 2010;92:2077–2082.
[16] Almeida FS, Awruch AM. Design Optimization of Composite Laminated Structures Using Genetic Algorithms and Finite Element Analysis. *Compos Struct* 2009;88:443–454.
[17] Alonso MG, Duysinx P. Particle Swarm Optimization (PSO): an Alternative Method for Composite Optimization. *10th World Congress on Structural and Multidisciplinary Optimization* 2013:1–10.
[18] Chen J, Tang Y, Ge R, An Q, Guo X. Reliability Design Optimization of Composite Structures Based on PSO Together with FEA. *Chinese J Aeronaut* 2013;26:343–349.
[19] Sharma DS, Patel NP, Trivedi RR. Optimum Design of Laminates Containing an Elliptical Hole. *Int J Mech Sci* 2014;85:76–87.
[20] Zhu X, He R, Lu X, Ling X, Zhu L, Liu B. A Optimization Technique for the Composite Strut Using Genetic Algorithms. *Mater Des* 2015;65:482–488.
[21] Jafari M, Rohani A. Optimization of Perforated Composite Plates under Tensile Stress Using Genetic Algorithm. *J Compos Mater* 2016;50:2773-2781.
[22] Kennedy J, Eberhart R. Particle Swarm Optimization. *Proc. ICNN'95 - Int. Conf. Neural Networks, vol. 4, IEEE* 1995 p. 1942–1948.
[23] Yang X, Yuan J, Yuan J, Mao H. A Modified Particle Swarm Optimizer with Dynamic Adaptation. *Appl Math Comput* 2007;189:1205–1213.
[24] Talbi EG. Metaheuristics: From Design to Implememntation Hoboken, *NJ, USA: John Wiley & Sons, Inc.*; 2009.
[25] Chan F, Tiwari MK. Swarm Intelligence: Focus on Ant and Particle Swarm Optimization. *Vienna, Austria, I-Tech Education and Publishing,* 2007.
[26] Ratnaweera A, Halgamuge SK, Watson HC. Self-Organizing Hierarchical Particle Swarm Optimizer With Time-Varying Acceleration Coefficients. *IEEE Trans Evol Comput* 2004;8:240–255.
[27] Ukadgaonker VG, Rao DKN. A General Solution for Stresses Around Holes in Symmetric Laminates under In-plane Loading. *Compos Struct* 2000;49:339–354.